Electrochimica Acta, Vol. 35, No. 11/12, pp. 1787–1795, 1990
Printed in Great Britain

0013-4686/90 $3.00 + 0.00
Pergamon Press plc

EFFECT OF ELECTRODE MATERIAL ON $SOCl_2$ REDUCTION

P. A. MOSIER-BOSS and S. SZPAK
Naval Ocean Systems Center, San Diego CA 92152-5000, U.S.A.
J. J. SMITH
Department of Energy, Washington DC 20545, U.S.A.
and
R. J. NOWAK
Office of Naval Research, Arlington VA 22217-5000, U.S.A.

(*Received* 5 *September* 1989; *in revised form* 6 *February* 1990)

Abstract—The effect of electrode material on the elementary processes associated with the electroreduction of the $SOCl_2$–$AlCl_3$ system is examined by three techniques: *ir*-reflectance spectroscopy, linear scan voltammetry and galvanostatic pulsing. The results of spectroscopic examination indicate the same reaction path, *ie* independent of electrode material, while the shape of voltammograms clearly show the effect of electrode material on the reaction kinetics. The latter result is further supported by galvanostatic pulse experiments.

Key words: $SOCl_2$ electroreduction, *ir*-reflectance spectroscopy, electrode material

NOMENCLATURE

c	concentration, mol cm^{-3}
C	capacitance, As V^{-1}
D	diffusion coefficient, cm^2 s^{-1}
E	potential, V
F	Faraday constant, 96487 C mol^{-1}
j	current density, A cm^{-2}
k	rate constant, defined in Fig. 4
l	running index
m	running index
n	running index
R	gas constant, J K^{-1} mol^{-1}
t	time, s
T	temperature, K
x	coordinate, cm
Γ_m	maximum surface concentration, mol cm^{-2}
η	overpotential, V
θ	surface coverage
λ	parameter, defined in 3.2.1
ξ	parameter, defined in 3.2.1

1. INTRODUCTION

A technologically important $Li/SOCl_2$ electrochemical power source, exhibiting a high theoretical energy density, was discovered in the late 1960s and reduced to practice, for low discharge rates in the 1970s. A decade later a new requirement was imposed, that of maximizing its power density. To accomplish this, two design approaches were suggested: the construction of a module containing in-series connected thin cells, as one choice, and the employment of a flowing electrolyte, as the other. Seeking an improvement in performance in each of the proposed designs, modifications of both the electrode structure and composition were undertaken, unfortunately, with mixed results. Some of the difficulties were resolved through cell modeling. The conclusions reached by Tsaur and Pollard[1], Smith *et al.*[2] and Nowak *et al.*[3] showed that, in general, good agreement exists between the theory and practice and that the important factor in determining the cell lifetime is the form of the local current density–overpotential relation and the ensuing changes associated with the reaction path. Examination of this system by cyclic voltammetry indicated a complex reaction path suggesting that more than one species participates in the charge transfer process, *via* an adsorption step[4, 5]. Consequently, information on the form and content of the polarization equation and the structure and properties of the electrolyte and the electrode-electrolyte interphase, are of immediate interest.

In this communication, we examine the effect of electrode material on the form of the $j = j(\eta)$ relationship. We limit the discussion to events occurring at Au and C-glassy and, to a lesser degree Si, electrode surfaces; the smooth Pt electrode is used as the standard for comparison. Emphasis is on the qualitative aspects of the charge transfer process. Subject to geometrical constraints, the events occurring on smooth surface describe the behavior of the porous structure found in practical batteries[6].

2. EXPERIMENTAL

Experimental details were presented elsewhere [7, 8]. Here, for convenience, we provide a brief summary only.

2.1. *Materials/procedures*

An analytical grade of thionyl chloride was distilled and the middle fraction was collected and stored under argon. C.P. grade aluminum chloride and lithium chloride were used as received. All solutions were prepared in a glove bag in an inert atmosphere

of Ar by dissolving known amounts of Al_2Cl_6 and LiCl in $SOCl_2$.

2.2 *Electrode preparation*

Before each experiment, the Pt, C-glassy and Au working electrodes were polished with an Al_2O_3 aqueous slurry on a polishing cloth. After rinsing with water the electrodes were sonicated for 5 minutes to remove residual alumina particles. After a second aqueous rinse, Au and Pt electrodes were rinsed with methanol and allowed to air dry. After sonication, the C-glassy electrode was rinsed with 0.05 M H_2SO_4 followed by an aqueous rinse and a methanol rinse. In the voltammetry and glavanostatic pulsing experiments the areas of the electrodes are 0.181 cm^2 for Pt and Au and 0.071 cm^2 for C-glassy. The electrodes were of the same degree of roughness.

2.3 *Instrumentation*

The *ir* spectra were obtained on a Nicolet 5 DXB FT-*ir* spectrometer (with a resolution of 2 cm^{-1}). The external reflectance spectro-electrochemical cell, patterned after that of Foley and Pons[9], was constructed from a machineable ceramic material and provided with a variable distance between the AgCl window and the working electrode surface. The potential time sweep rate and the electrode galvanostatic pulsing were controlled by a computer driven potentiostat, PAR model 173, with a 276 IEEE computer interface.

3. RESULTS AND DISCUSSION

3.1 *Methodology*

The electroreduction of $SOCl_2$ in practical batteries, as well as on smooth electrode surfaces, comprises a set (perhaps more than one set) of consecutive processes occurring within the interphase region. The analysis of these processes, given in Ref.[5], is based on the van Rysselberghe concept of the interphase region[10], which is based on an open system whose structure is generated by, and responds to, the demands imposed by the dominating process(es). This concept is retained and, when coupled with three experimental techniques, *viz. ir* spectroscopy, cyclic voltammetry and galvanostatic pulsing, is used to illustrate the effect of the electrode material on the charge transfer process, its mechanism and kinetics.

3.1.1 *Infra-red spectroscopy. In situ* reflectance *ir* spectroscopy is a powerful tool in probing the electrode/electrolyte interphase[11]. By varying the electrode potential, it is possible to determine, from changes in the spectra, the species undergoing electroreduction as well as their orientation on the electrode surface. However, before such experiments can be correctly interpreted, a thorough understanding is necessary regarding the species present in the bulk solution and the equilibria between them. The examination of the LiCl–$AlCl_3$–$SOCl_2$ tenary system[7, 8] revealed that: (i) $SOCl_2$ is a weakly associated liquid, (ii) Al_2Cl_6 dissolves dissociatively with the formation of a 1 : 1 adduct, $Cl_3Al{\leftarrow}OSCl_2$; (iii) these adducts undergo an internal exchange reaction to form $AlCl_4^-$ and onium ion, $[Cl_2(O{=})S{\rightarrow}Al{\leftarrow}OSCl_2]^+$, and (iv) the addition of LiCl breaks up the adduct and onium ion to form $AlCl_4^-$ and solvated Li^+ ion, $Li(\leftarrow OSCl_2)_3^+$.

Of interest in the analysis of the electrode/electrolyte interphase is the spectral region 925–1400 cm^{-1} where the S–O stretching vibrations of neat $SOCl_2$, solvated Li^+ ion, adduct and onium ion occur at 1231, 1202, 1117 and 1065 cm^{-1}, respectively. Within this region, the S–O vibrations, which are very sensitive to any changes in the molecular structure, are not obstructed by other absorptions[7]. A typical spectrum of the Au/$SOCl_2$, $AlCl_3$ interphase is shown in Fig. 1. It reveals the preferential adsorption on the electrode surface and enrichment within the interphase of both onium ions and 1 : 1 adducts. This enrichment can be demonstrated in two ways; by using a polarized beam or by varying the spacing between the electrode and window[5]. For practical reasons, the latter has been employed. The de-convolution of the bands into Voigt profiles, shown in Fig. 1, provides additional information on the composition of the interphase. Besides the two bands due to adduct and onium ion, two additional bands appear at 1132 and 1102 cm^{-1}. These two bands, which disappear upon cathodic polarization, were tentatively assigned earlier as either (i) the symmetric and asymmetric vibrations of the adsorbed onium ion or (ii) the S–O stretching vibrations of onium ion and adduct, respectively[5]. The most probable assignment is to the adsorbed onium ion. Reduction of the onium ion occurs as the initial step in the overall reduction process and may well be the only species directly reduced (*vide infra*). The disappearence of the 1132 and 1102 cm^{-1} peaks on polarization appears to be coupled suggesting that they are derived from the same species. The shift to higher frequency indicates that adsorption is through the S atom[5].

3.1.2 *Cyclic voltammetry.* Mosier-Boss *et al.*[5] postulated a set of events comprising the charge transfer process which is represented by the scheme:

$$\ldots R(d) \rightarrow R(r) \rightarrow R(a) + e^- \rightarrow P_1(a) + e^- \rightarrow P_2(a) \rightarrow \ldots \quad (1)$$

Reacting molecules, R(d), are brought to the electrode surface through the reaction zone, (r), by diffusion. The adsorption molecules, R(a), undergo the charge transfer, accepting one or more electrons, yielding products $P_1(a)$, $P_2(a)$, ... The reaction layer is formed when the product species interact with the oncoming R molecules. This layer is sandwiched between the diffusion and adsorption layers thus constructing an interphase region consisting of a number of layers populated by the interacting species. This type of system has been examined by, among others, Saveant and Vianello[13]. In such systems, the current time dependence $i(0, t)$, for a charge transfer process involving N electroactive species and M adsorption process, is given by equation (2):

$$i(0, t) = F\left[\sum_{n=1}^{N} z_n D_n \frac{\partial c_n}{\partial x} + \sum_{m=1}^{M} \Gamma_m \frac{d\theta_m}{dt}\right] \quad (2)$$

The right-hand side of equation (2) accounts for contributions due to diffusional flux (*via* the sum of concentration gradients and the kinetics of adsorption, expressed in terms of the change in the surface

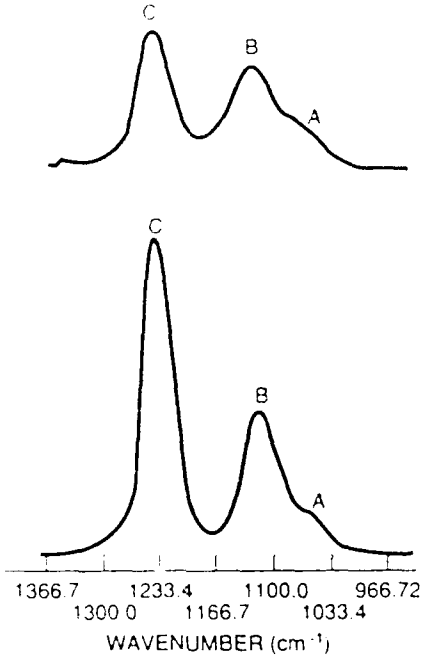

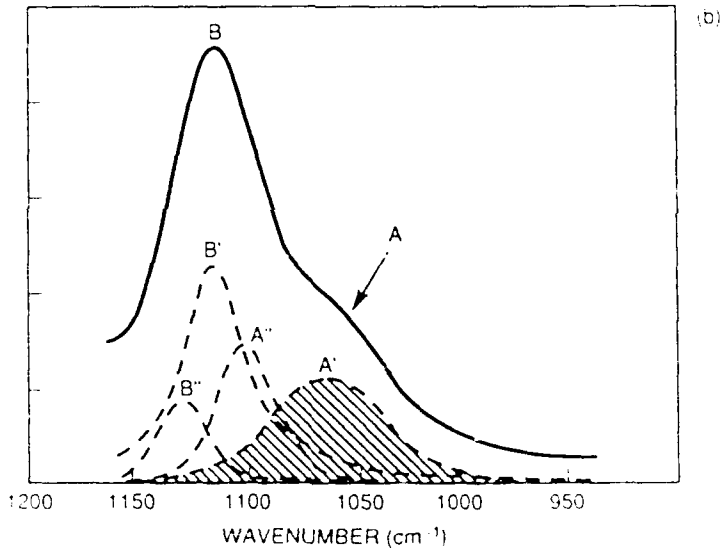

Fig. 1. The 930–1350 cm^{-1} ν spectra region (system: Au $SOCl_2$–$AlCl_3$). (a) Effect of cell path length (upper) 5 μm, (lower) 10 μm. S–O stretching vibrations: (A) in onium ion at 1065 cm^{-1}, (B) in 1 : 1 complex at 1117 cm^{-1}, (C) in neat $SOCl_2$ at 1228 cm^{-1}. (b) Decomposition of A and B bands into Voigt profiles. A' and B' for species in bulk solution, A'' and B'' for adsorbed species at 1065, 1117, 1133 and 1102 cm^{-1}, respectively.

concentration summed over the number of adsorption processes. The concentration gradient(s) of the electroactive species is obtained from the mass balance equation

$$\frac{\partial C_m}{\partial t} = D \frac{\partial^2 C_m}{\partial x^2} + f_m(\xi, \lambda), \qquad (3)$$

which is solved subject to boundary conditions reflecting the experimental constraints. The function, $f_m(\xi, \lambda)$, is formulated for a specific set of events occurring within the interphase in the course of charge transfer. In particular, ξ refers to thermodynamic aspects, *eg* equilibria between species populating the interphase, while λ contains information on the rate of relevant processes, including the forcing perturbation, *eg* potential scan rate. An example of the effect of kinetic factors on the voltammogram is illustrated in Fig. 2. In particular, a change in the forcing function, through the ν-parameter, affects the reducing current of the voltammogram more than its oxidizing current. Moreover, certain characteristic features of the interphase response to potential per-

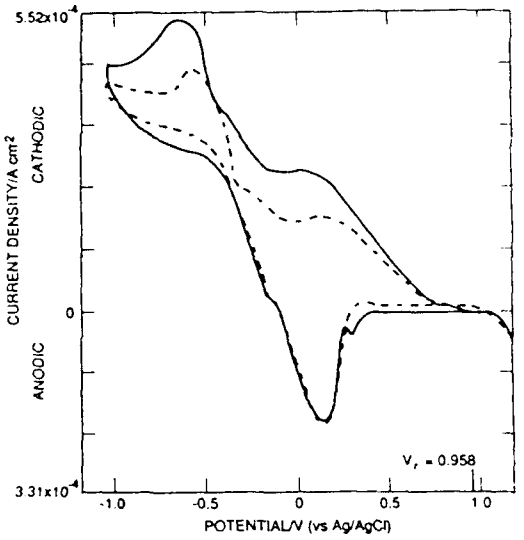

Fig. 2. Effect of scan rate on voltammogram shape. System: $Pt/SOCl_2$–3.0 M $AlCl_3$; solid line; $v = 10\ mV\ s^{-1}$; dashed; $5\ mV\ s^{-1}$

turbation, *eg* autocatalysis, adsorption and desorption, are more sharply defined at lower scan rates.

3.1.3. *Galvanostatic pulsing*. Additional information can be extracted by changing the nature of the forcing function, $f_n(\xi, \lambda)$. For a class of electrode process where adsorbed species dominate, the electrode potential can be written in a general form:

$$E = E(\theta_1, \theta_2, \ldots; f), \tag{4}$$

and its time dependence can be obtained by formal differentiation which, for a galvanostatic pulse, yields equation (5):

$$\frac{dE}{dt} = \sum_n \left.\frac{\partial E}{\partial \theta_i}\right|_{j,n \neq i} \frac{d\theta_i}{dt}. \tag{5}$$

Equation (5) indicates that, for $n > 1$, only rarely should a constant potential be observed during charge transfer because of the accumulation of adsorbed species. It is of interest to note, however, that equation (5) applies also on interruption of current; it follows, therefore, that qualitative information concerning the number of adsorbed species and the relative magnitude of the respective rate constants may be inferred from the examination of $E(t)$ measured across the relaxing interphase. An example of the electrode potential response to a 0.0011 A cm^{-2} galvanostatic pulse and the return to rest potential is shown in Fig. 3. The changing conditions on the electrode surface are clearly displayed.

3.2. *Reaction path*

Most recently, Mosier-Boss *et al.*[12] examined the *ir* spectra and linear scan voltammetry in greater detail. The rather crude formulation of the reaction scheme, equation (1) was refined to include additional activities, *viz.* desorption processes and catalytic events, illustrated in Fig. 4. In Fig. 4, A_0, A_1 and A_1^+ refer to neat $SOCl_2$, 1 : 1 complex and onium ion, respectively. The reformulated reaction scheme shows clearly the interplay between the thermodynamic and kinetic aspects of the $SOCl_2$ reduction on the electrode surface. This representation also aids in the interpretation of experimental data, especially when such data are obtained under transient conditions. The effect of the electrode material will enter through the kinetically controlled part of the overall process, denoted as the λ-region and, only peripherally involving thermodynamic considerations contained within the ξ-region. Thus, the effect of electrode material will appear as a change in the rate constant of the process in the adsorbed state.

3.2.1. *Infrared spectra: species present*. Determination of the effect of electrode materials on the

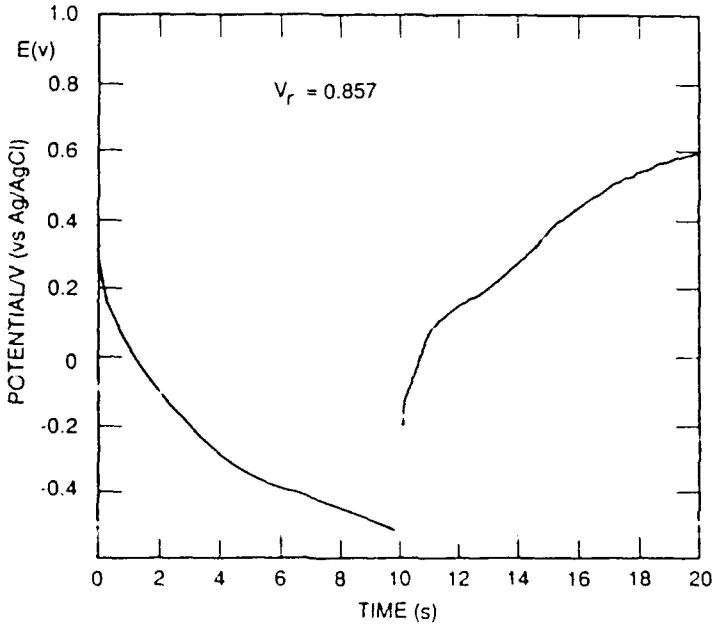

Fig. 3. Potential–time behavior across charging and relaxing interphase. System: $Pt/SOCl_2$–3.0 M $AlCl_3$–0.1 M LiCl; pulse current 0.0011 A cm^{-2}.

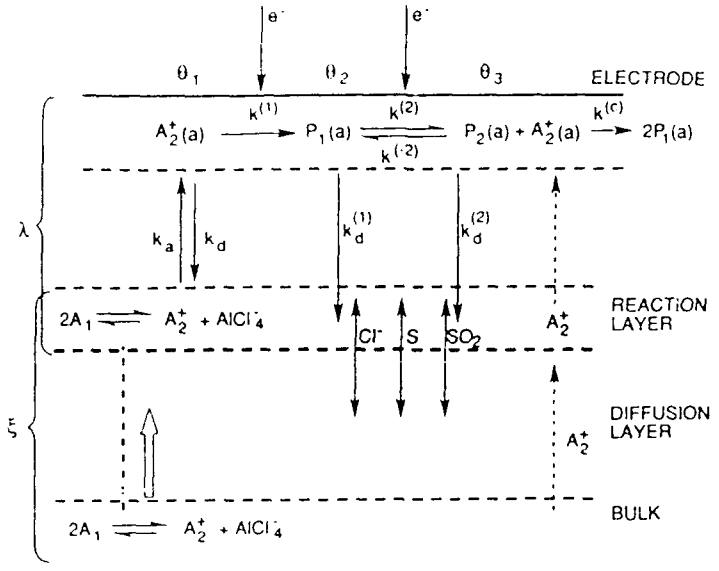

Fig. 4. Summary of $SOCl_2$ reduction path. System: $AlCl_3$–$SOCl_2$; processes affecting the ξ and λ components of the forcing function $f_n(\xi, \lambda)$ indicated. Rate constants identified.

reduction of $SOCl_2$-bearing species by the potential perturbation technique requires that the reaction path remains unchanged. The constancy of the reaction path is manifested by identical species populating the electrode/electrolyte interphase, *ie* irrespective of the electrode material. To ascertain this, the spectral region 925–1400 cm^{-1} was examined by *in situ ir* spectroscopy for each electrode material.

Figures 5a–d show this region reflected from the Au-, Pt-, *n*-Si- and C-glassy surfaces at rest potential (dashed lines) and while cathodically polarized (solid lines). It is seen that the species present on and near the surface are the same regardless of the electrode material which, in turn, indicates that the reduction path is the same on metallic and semiconducting surfaces. It is also seen that the concentration of reactant(s) and product(s) within the interphase differs which is expected because adsorption phenomena are highly specific. In particular, at low overpotentials the major event is the potential dependent shift in equilibria between the $SOCl_2$- bearing species, *eg* onium ion and adduct, occurring within the confines of the interphase region. With a further increase in overpotential, new peaks appear at 1331, and *ca* 1150 cm^{-1} due to the formation of SO_2 and at 1190 and 1170 cm^{-1} assigned to, as yet, unidentified intermediate species containing S–O bond(s). Concurrently, there is a loss in the concentration of the 1 : 1 adduct, as well as the onium ion. From the *in situ ir* spectroscopy it is not clear whether both the onium ion and 1 : 1 adduct are simultaneously reduced or if only one species participates in the charge transfer process. This ambiguity exists because the onium ion and the 1 : 1 adduct are coupled to one another *via* a chemical equilibrium. Additional experimental techniques must be sought to resolve this ambiguity.

3.2.2. *Linear scan voltammetry: rate constants.* Equations (2) and (3) indicate that certain conditions must be met to show the effect of electrode material: one is the specified scan rate, as illustrated in Fig. 2, the other is the composition of the bulk phase, Figs 6a and b. It is seen that the change in the composition *eg* by addition of iron phthalocyanine or an increase in $AlCl_3$ concentration substantially changes the shape of the voltammograms.

Earlier[5], we concluded that the electroreduction of $SOCl_2$ is a two-electron transfer in which the first one, equation (6) is irreversible and the second equation (7), is quasi-reversible

$$A_2^+ + e^- \rightarrow P_1, \tag{6}$$

$$P_1 + e^- \rightarrow P_2. \tag{7}$$

P_1 and P_2 are intermediate species which desorb from the electrode surface into the reaction layer where they react with other species to form the products of electroreduction Cl^-, S, SO_2. The charge transfer reactions, equations (6) and (7) can be cast into corresponding rate equations. To illustrate, the rate of the charge transfer involving the first electron, neglecting diffusion, is:

$$\Gamma_m \frac{d\theta_i}{dt} = k_a c_{A_2^+}(1 - \sum \theta_i)F - k_d\theta_i - k^{(1)}\theta_i \times \exp(\alpha F\eta_1/RT) - k^{(c)}\theta_i\theta_3,$$

$$\eta = E - E_{rev}, \tag{8}$$

with similar statements for the time change in other adsorbed species. The rate constants and θ's are defined in Fig. 4. The right-hand side contains the rate constants k_a, $k^{(1)}$, $k^{(c)}$ and k_d for the adsorption, electron transfer, autocatalysis and desorption processes. Equation (8) then accounts for the various processes experienced by the reacting molecules as they traverse the interphase, *cf.* Fig. 4 for notation. Depending on conditions of concentration, applied potential and surface coverage, the relative importance of the terms in equation (8) will change.

It is known[13] that, for a given set of experimental constraints, the linear scan voltammetry delineates

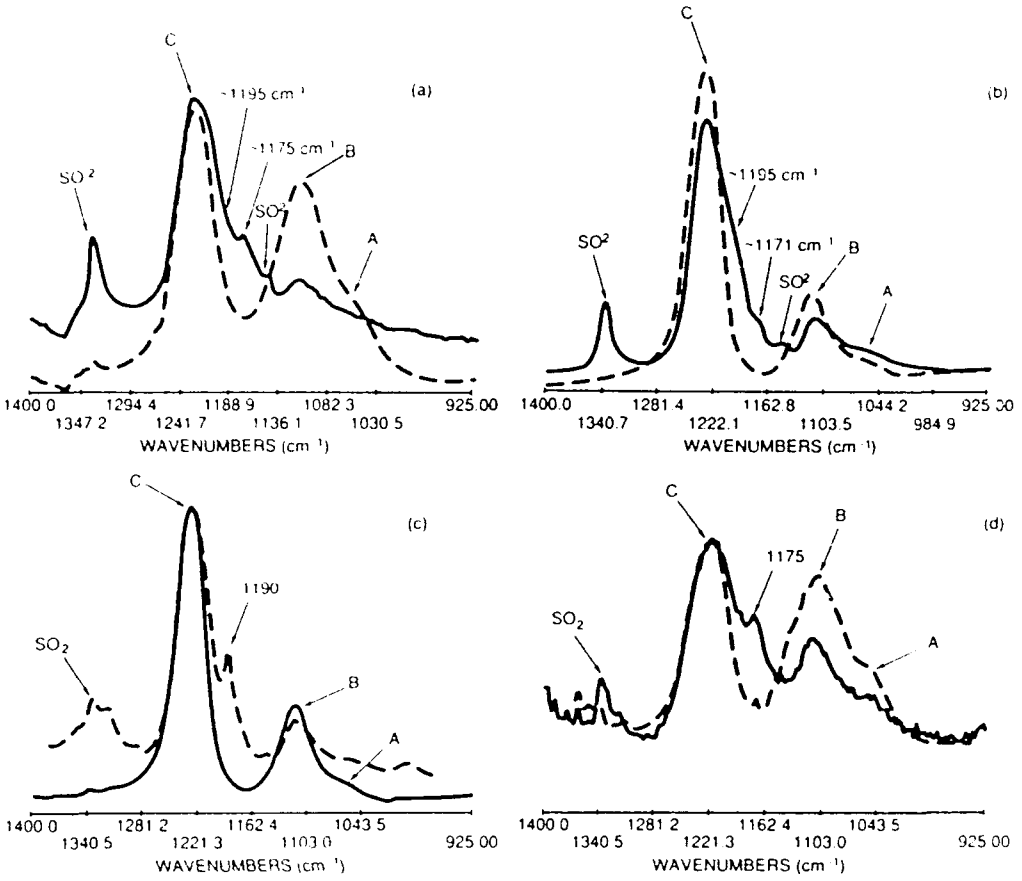

Fig. 5. Effect of applied potential and electrode material on *ir* reflectance spectrum. Spectral region: 925–1400 cm^{-1}. System: Me 3.0 M $AlCl_3$–$SOCl_2$, (a), (b), (c) and (d) reflected from Au, Pt, Si and C-glassy electrode surface, respectively. Dashed line: electrode at rest potential. Solid line: polarized to −2.5 (Au), −3.5 (Pt), −3.0 (Si) and −2.0 V (C-glassy). Bands A, B and C refer to onium ions, 1 : 1 complex and neat $SOCl_2$ in the bulk solution, respectively.

regimes of the dominance of specific processes. In the present case, constraints applied in Fig. 2 produced a balanced set, *ie* where no single process dominates the voltammogram. Thus, the presence of a current plateau, which is associated with the first electron transfer, suggests a coupled chemical reaction either preceding or parallel with the charge transfer. Indeed, an equilibrium does exist between onium ion and 1 : 1 adduct and, from the *in situ ir* experiments, we observe a loss of both of these species with increasing overpotential[5]. Changing the composition of the electrolyte phase by either increasing the $AlCl_3$ concentration, Fig. 6a, or by the addition of a small amount of Fe-Pc (*eg* 2 mg cm^{-3}), Fig. 6b substantially alters the shape of the voltammogram, *vide supra*, Fig. 2. In the first case, as we increase the concentration of $AlCl_3$, and thus, the concentration of onium ions, an auto-catalytic effect, manifested by a cross-over behavior, is observed. Moreover, since the cross over point occurs at the juncture between the plateau and the cathodic peak at all scan rates, the species being regenerated on the electrode surface, *via* equation (9) is P_1

$$P_2 + A_1^+ \rightarrow 2P_1 \qquad (9)$$

Addition of Fe-Pc, to the electrolyte solution produces a voltammogram indicative of a catalytic effect[14, 15]. The catalysis masks contributions due to strongly adsorbed species, the coupled chemical equilibrium and the charge transfer. In terms of the reaction path illustrated in Fig. 4, the addition of $AlCl_3$ has no effect on any rate constant—the auto-catalytic effect enters through an increase in the concentration of A_1^+ (a) while in the second case (Fe-Pc addition), the $k^{(1)}$ is faster for the $Pt/SOCl_2$-(Fe-Pc) than for $Pt/SOCl_2$. This is not the only effect, however: since the anodic peak due to the re-oxidation of $P_2 \rightarrow P_1$ is less prominent, the rate constant, $k^{(c)}_{Fe\text{-}Pc}$, is increased in the presence of dissolved Fe-Pc.

The effect of the electrode material on the rate constant is illustrated in Figs 7a–c. In particular, Fig. 7a shows the effect of surface modification of the Pt-electrode by a chemisorbed Fe-Pc. Comparison of voltammograms in Figs 2 and 7a shows a significant increase in the rate of the charge transfer associated with the first electron, *ie* $k^{(1)}_{Pt/Fe\text{-}Pc} > k^{(1)}_{Pt}$ and similarly notable reduction in the second peak can be interpreted as an increase in the $k^{(c)}$-value. It is unlikely that any of the features of the cyclic voltammograms

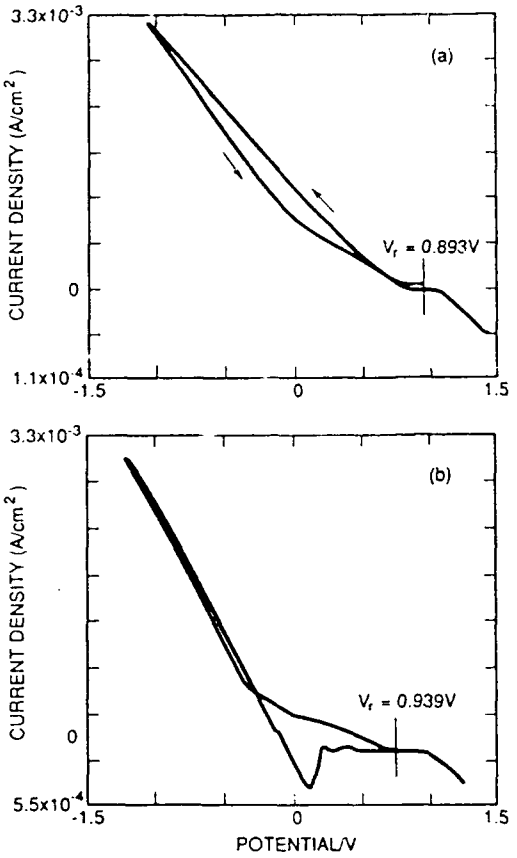

Fig. 6. Effect of solution composition on linear scan voltammogram. System: $Pt/SOCl_2$–$AlCl_3$; scan rate 10 mV s^{-1}. (a) 3.0 M $AlCl_3$ in $SOCl_2$ with added 2.0 mg cm^{-3} Fe–Pc; (b) 4.0 M $AlCl_3$ in $SOCl_2$.

is due to the reduction of the central metal ion of Fe–Pc. No such waves were observed in Fig. 6a nor has any such process been observed by Melendres *et al.*[16,17]. The voltammogram on Au-surface, Fig. 7b, shows a substantial increase in the $k^{(1)}$-rate constant, thus obscuring the contributions due to adsorption. On a glassy C surface, Fig. 7c, we note a substantial auto-catalytic effect only. The auto-catalytic effects are associated with the process described by equation (9) coupled with relevant equilibria.

3.2.3. *Relaxation of interphase: accumulation of adsorbed species.* An interpretation of the potential decay curves in terms of equation (5) involves the evaluation of both $\partial E/\partial\theta$ and $d\theta/dt$. Invoking the Faraday law only, *ie* neglecting the mass transport term in equation (2), we have $d\theta_i/dt = j_{f,i}F\Gamma_{m,i}$ which, upon substitution into equation (5) yields:

$$\frac{dE}{dt} = \sum_n \frac{\partial E}{\partial \theta_i}\bigg|_{j,t,\neq n} \left(\frac{j_{f,i}}{F\Gamma_{m,i}}\right). \tag{10}$$

On the other hand[18], a general expression for the electrode response to, *eg*, pulse current j_{ex}, is:

$$C\frac{dE}{dt} = j_{ex} - \sum_n j_{f,n}. \tag{11}$$

By comparing equations (10) and (11), we have $\partial E/\partial\theta = F\Gamma_m/C$. Thus, as a first approximation we take $\partial E/\partial\theta$ = const and examine changes in the $E(t)$-curves in terms of partial faradaic currents, *ie* we attempt to assign the observed change in the mode of interphase relaxation to a particular process.

The potential–time behavior of the electrode response to galvanostatic pulse and during its return to the rest potential, shown in Fig. 3, is in general agreement with the reaction path in Fig. 4, *vide infra*. (The low concentration of LiCl present in the electrolyte did not significantly alter the shape of the curves.) In what follows, results of two sets of experiments are presented, *viz.*, the effect of pulse current density and the effect of pulse length on the shape of the $E(t)$ curves are examined. As an example, we have selected

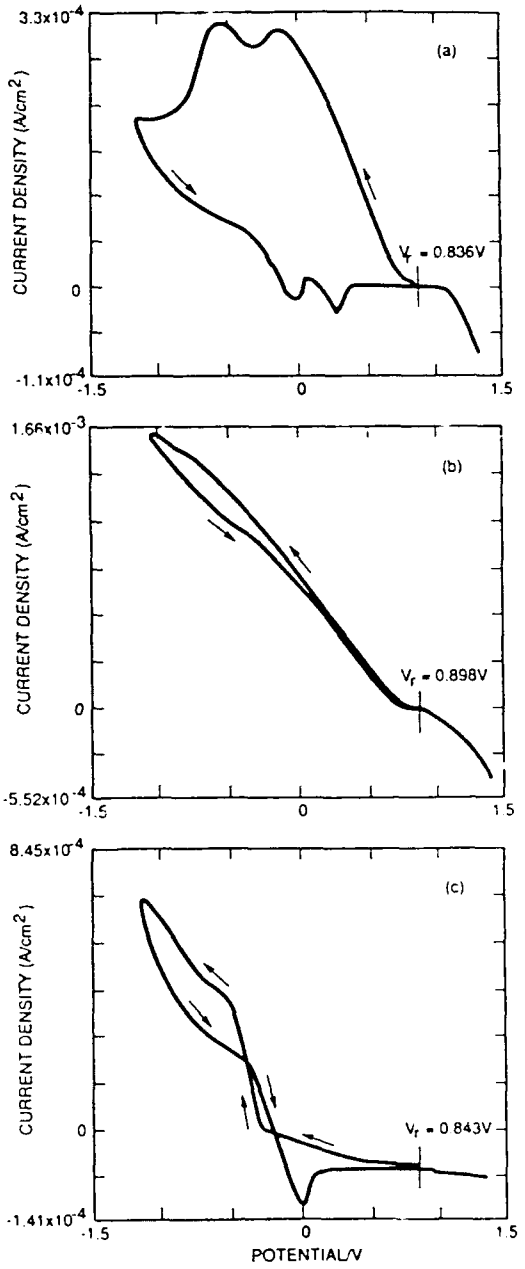

Fig. 7. Effect of electrode material on linear scan voltammogram. System: Me/3.0 M $AlCl_3$ in $SOCl_2$; scan rate 10 mV s^{-1}. (a) Pt electrode with chemisorbed Fe–Pc; (b) Au electrode; (c) glassy C electrode.

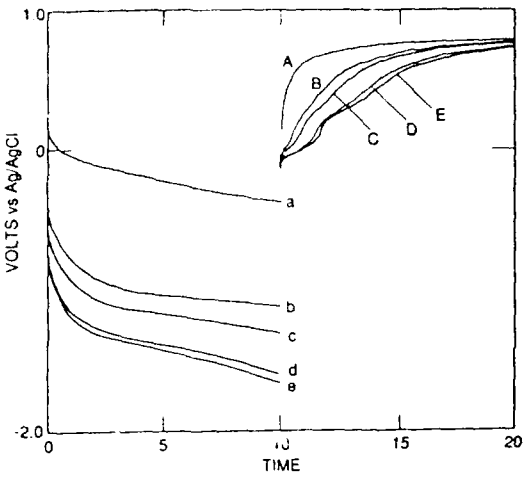

Fig. 8. Potential-time behavior as a function of pulse strength. System: glassy C/2.0 M $AlCl_3$.

the Pt/... system to illustrate the effect of pulse strength, Fig. 8, and the C-glassy /... to display the change in electrode potential upon a return to the initial state, following varying pulse length, Fig. 9.

The development of characteristic features of the $E(t)$ decay curves with either pulse strength or its duration, indicates the accumulation of reaction products within the interphase. This accumulation becomes clearly evident as more charge is forced across the interphase. Qualitatively, the more charge that crosses the interphase, the more pronounced the complexity of the potential decay curve. For a small amount of charge transferred (*ie* short pulsing time or low pulse current), the $E(t)$ curve is almost exponential, as could be expected from integration of equation (5) for one process determining the electrode potential which would yield:

$$e^{(E_0 - E)/b} - 1 + \frac{j(0)t}{bC}\ ;\ b = RT/F. \qquad (12)$$

At a somewhat longer current pulse, the potential decay curve develops an inflection and can be approximated by two exponential decays. With further increase in the pulse duration, the inflection point becomes a straight line with its slope and length proportional to the pulse duration. In general, the number of exponential decays observed in the potential relaxation curve reflects the number of adsorbed species[15]. The shape of these decay curves is determined by the potential determining processes while the rate of the accumulation of reaction products is the result of the magnitude of rate constants of the partial process illustrated in Fig. 4. Thus, it is expected that, for the same pulse duration, the degree of accumulation will depend on the electrode material. For example, with the passage of time at both Pt and C-glassy, a composition of the interphase is reached such that three exponentially decaying segments can be seen. This is indicative of three adsorbed species being presented, *viz.*, A_2^*, P_1 and P_2. On the other hand, for the relaxing Au/$SOCl_2$–$AlCl_3$ or the Pt/$SOCl_2$–$AlCl_3$(Fe–Pc) interphases only one exponential decay, characteristic of a strong catalytic effect, is observed.

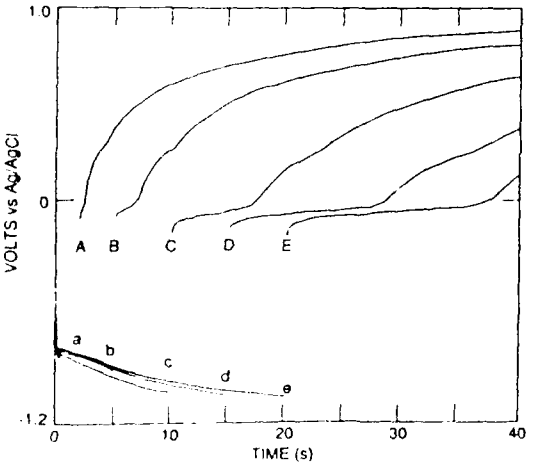

Fig. 9. Potential-time behavior as a function of pulse duration. System: Pt/3.0 M $AlCl_3$.

4. CLOSING REMARKS

The complexity of the reaction path, equation (1) or Fig. 4, indicates that the material employed in the construction of the positive electrode might affect the performance of a discharging Li/$SOCl_2$ cell. The primary reason for such a conclusion is the presence of adsorbed species whose adsorption–desorption rates, as well as catalytic activities, depend on the electrode material. The experimental approach involved the identification of adsorbed species by *ir* reflectance spectroscopy of an electrode–electrolyte interphase at rest and when cathodically polarized. Examination of the 925–1400 cm^{-1} spectra region revealed that the surface concentrations of adsorbent molecules, but not their chemical nature, were affected by the electrode material. This is, of course, an expected result because of the specificity of adsorption.

The shape of the linear scan voltammetry is determined solely by the mass balance equation, equation (3), through the forcing function $f_n(\xi, \lambda)$ with ξ reflecting the thermodynamics and λ the kinetics of the system. The examination of the voltammogram shape as a function of electrode material, for an *a priori* selected set of experimental conditions, led to the following relations:

$$k_{Au}^{(1)} > k_{Pt(Fe\text{-}Pc)}^{(1)} > k_C^{(1)} \qquad (13)$$

$$k_{Au}^{(c)} > k_C^{(c)} > k_{Pt}^{(c)}. \qquad (14)$$

This series in rate constants is further supported by the potential decay across the relaxing electrode–electrolyte interphases.

Acknowledgement—This work was, in part, supported by the Office of Naval Research, Arlington, VA.

REFERENCES

1. K. C. Tsaur and R. Pollard, *J. electrochem. Soc.* **133**, 2296 (1986).

2. J. J. Smith, S. Szpak and W. A. West, in *Power Sources 11* (Edited by L. J. Pearce), International Power Sources Symposium, Brighton, U.K. (1987).
3. R. J. Nowak, D. R. Rolison, J. J. Smith and S. Szpak, *Electrochim. Acta* **33,** 1313 (1988).
4. M. J. Madou, J. J. Smith and S. Szpak, *J. electrochem. Soc.* **134,** 2794 (1987).
5. P. A. Mosier-Boss, S. Szpak, J. J. Smith and R. J. Nowak, *J. electrochem. Soc.* **134,** 2455 (1989).
6. S. Szpak, in *Techniques for Characterization of Electrodes and Electrochemical Processes* (Edited by R. Varma and J. R. Selman), Wiley, New York (1989).
7. P. A. Mosier-Boss, R. D. Boss, C. J. Gabriel, S. Szpak, J. J. Smith and R. J. Nowak, *J. chem. Soc. Faraday Trans.* **I, 85,** 11 (1989).
8. P. A. Mosier-Boss, S. Szpak, J. J. Smith and R. J. Nowak, *J. electrochem. Soc.* **136,** 1282 (1989).
9. J. K. Foley and S. Pons, *Anal. Chem.* **57,** 945A (1985).
10. P. van Rysselberghe, *Thermodynamics of Irreversible Processes*, Hermann, Paris (1963).
11. K. Ashley and S. Pons, *Chem. Rev.* **88,** 673 (1988).
12. P. A. Mosier-Boss, S. Szpak, J. J. Smith and R. J. Nowak, Ext. Abstr. # 345, Electrochemical Society Spring Meeting, Los Anglees, CA (1989).
13. J. M. Saveant and E. Vianello, *Electrochim. Acta* **13,** 629 (1967).
14. R. S. Nicholson and I. Shain, *Anal. Chem.* **36,** 706 (1964).
15. R. H. Wopschall and I. Shain, *Anal. Chem.* **39,** 1514 (1967).
16. C. A. Melendres and F. A. Cafasso, *J. electrochem. Soc.* **128,** 755 (1981).
17. C. A. Melendres, C. B. Rios, X. Feng and R. McMasters, *J. phys. Chem.* **87,** 3526 (1983).
18. P. C. Milner, *J. electrochem. Soc.* **107,** 343 (1960).
19. B. E. Conway and M. Dziechiuch, *Can. J. Chem.* **41,** 21, 38, 55 (1963).